Proceedings of the 16th European VLBI Network Symposium
Ros, E., Benke, P., Dzib, S., Rottmann, I., & Zensus, J.A. (eds.)
September 2nd-6th 2024, Bonn, Germany

VLBI Observations of Dual AGNs

W. Xu[1], L. Cui[1], T. An[2], J. Yang[3], H. Cao[4], L. C. Ho[5], X. Liu[1]

[1] Xinjiang Astronomical Observatory, CAS, 150 Science-1 Street, 830011 Urumqi, People's Republic of China
[2] Shanghai Astronomical Observatory, CAS, 80 Nandan Road, 200030 Shanghai, People's Republic of China
[3] Department of Space, Earth and Environment, Chalmers University of Technology, Onsala Space Observatory, SE-439 92 Onsala, Sweden
[4] Shangqiu Normal University, 298 Wenhua Road, 476000 Shangqiu, Henan, People's Republic of China
[5] Kavli Institute for Astronomy and Astrophysics, Peking University, 100871 Beijing, People's Republic of China

Abstract. Dual active galactic nuclei (AGNs) and supermassive black hole (SMBH) binaries are crucial for understanding galaxy and black hole co-evolution, especially during mergers. These systems provide insights into interacting SMBH dynamics, AGN activity triggering, and SMBH coalescence processes. We observed four confirmed kpc-scale dual AGNs in Stripe 82 region using VLBA at 5 GHz in multiple-phase-center mode, aiming to study their milliarcsecond-scale radio emission properties. We detected two pc-scale radio cores labelled J0051+0020B and J2300-0005A. The radio emission of the other six AGNs was resolved out in high-resolution imaging. Based on the pc-scale radio emission properties, we analyzed the 5 GHz radio emission origins in detail for each source. The multiband study revealed a possible systematic X-ray deficit in our small dual-AGN sample, which could be attributed to the tidally induced effect and possibly viewing angle effect. In addition, to help further validate the Vastrometry method on dual-AGN selection, we also proposed EVN+e-MERLIN observations to reveal the fine radio structures and spectral properties of two Varstrometry selected dual-quasar candidates with z>0.5. The outstanding sensitivity and high resolution of EVN are helpful in achieving our scientific goals.

1. Introduction

According to the galaxy hierarchical evolution theory, small galaxies assemble through mergers and interactions into progressively larger systems, eventually forming the massive galaxies and clusters we observe today (Springel et al. 2005). It is generally believed that each galaxy typically harbors a supermassive black hole (SMBH) at its center (Kormendy & Ho 2013). During galaxy mergers, tidal torques could trigger the accretion and feedback of central black holes and form dual active galactic nuclei (AGN) (Di Matteo et al. 2005). However, only a few dual AGNs have been confirmed through observations. Studying the emission properties of rare dual AGN can provide valuable insights into galaxy merging and black hole activations.

2. VLBA Observations of Four Radio-Selected Dual AGNs in Stripe 82 Region

Previously, Fu et al. (2015a) found a group of dual-AGN candidates in Stripe 82 region by radio observations and optical spectroscopy. The follow-up VLA C-band observations confirmed that four of the pairs were true dual AGNs (Fu et al. 2015b). These dual AGNs exhibit paired mJy-level compact morphologies and steep radio spectra, suggesting the presence of kpc-scale radio jets and black hole activity (Fig. 1 middle column). The separation in each pair is about 2.5∼4.6 arcsec, corresponding to about 4.1∼11.6 kpc.

We observed the four confirmed dual AGNs using VLBA at 5 GHz in February, 2018 (project code: BL255A/B), aiming to reveal their milliarcsecond-scale radio emission properties. Our observations used multiple-phase-center mode which allows high-resolution imaging of each AGN within the primary beam area by adjusting the phase center (Deller et al. 2011). In addition, the phase-referencing technique can provide the precise positions of central black holes (Beasley & Conway 1995). The observational data was calibrated in the NRAO Astronomical Image Processing System (AIPS; Greisen 2003) with traditional VLBA phase-referencing calibration process, and imaged in DIFMAP (Shepherd 1997) through Gaussian model fitting with natural weight.

Our VLBA 5 GHz observations detected two pc-scale radio cores labelled J0051+0020B and J2300-0005A (Figure 1 side columns). The radio emission of the other six AGNs was resolved out in high-resolution imaging. The VLBA imaging and model parameters are listed in Table 1 column (2)∼(5). We obtained the phase-referenced coordinates (Table 2) and 5 GHz flux densities of two VLBA-detected sources, and estimated their brightness temperatures and radio emission powers using formula (1)∼(2). Their pc-scale radio emission properties are similar to those of typical jet-dominated AGNs. For the other six undetected sources, we provided their upper-limit values of these parameters (Table 1 column (6)∼(9)). For J2206+0003B and J2300-0005B, due to the limitations of VLBA observational sensitivity, we use lower VLA 5 GHz flux densities as their upper limits.

Table 1. VLBI imaging and model parameters

Source	$S_{5\rm GHz}^{\rm Peak}$ [mJy/beam]	RMS [mJy/beam]	SNR	Beam size [mas×mas]	$S_{5\rm GHz}^{\rm VLBA}$ [mJy]	θ [mas]	log T_b [K]	log $L_{5\rm GHz}$ [W/Hz]
(1)	(2)	(3)	(4)	(5)	(6)	(7)	(8)	(9)
J0051+0020A	0.121	0.024	4.99	7.04×2.04	<0.146	>3.79	<5.74	<21.72
J0051+0020B	0.183	0.023	7.85	7.04×2.04	0.20±0.03	0.84±0.24	∼7.21	∼21.77
J2206+0003A	0.121	0.023	5.16	6.13×1.93	<0.140	>3.44	<5.78	<20.85
J2206+0003B	0.132	0.024	5.50	6.13×1.93	<0.110*	>3.44	<5.67	<20.75
J2232+0012A	0.139	0.026	5.33	6.24×2.04	<0.156	>3.57	<5.86	<22.35
J2232+0012B	0.156	0.026	5.98	6.24×2.04	<0.157	>3.57	<5.87	<22.35
J2300−0005A	0.248	0.024	10.07	6.33×2.06	0.40±0.05	2.37±0.18	∼6.64	∼22.49
J2300−0005B	0.147	0.026	5.64	6.33×2.06	<0.084*	>3.61	<5.57	<21.88

Columns (2)–(5): VLBA imaging parameters. Column (6): the flux densities or 6σ upper limits. For J2206+0003B and J2300-0005B marked '*', replace with their VLA 5 GHz flux-density upper limits. Column (7): fitted Gaussian component diameter (FWHM). For undetected sources, use $\theta = \sqrt{beam_1 \times beam_2}$ to represent their lower limits of sizes. Column (8): rest-frame brightness temperatures or the upper limits. Column (9): radio emission powers or the upper limits. (Xu et al. 2024)

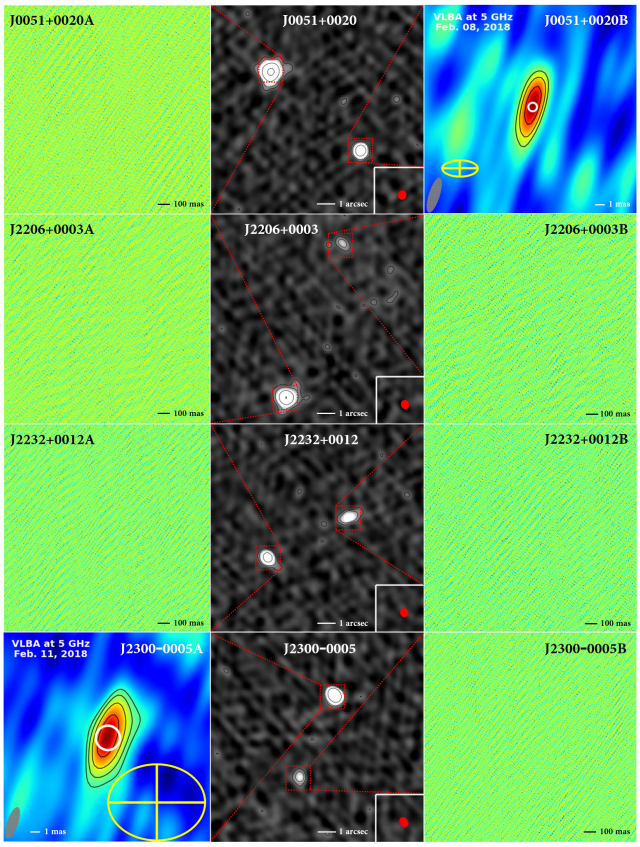

Fig. 1. Naturally weighted VLBA 5 GHz images (side columns) and VLA C-band images (middle column) of four dual AGNs (Xu et al. 2024). The black contours in the middle column are at (+3, +6, +24, +96)×σ (Fu et al. 2015b). For J0051+0020B and J2300-0005A, the final Gaussian fitting images with a scale of ±10 mas are provided, and the contours are at (+1, +$\sqrt{2}$, +2, +2$\sqrt{2}$)×3σ. The white circle in the center of the image is the circular Gaussian model. The yellow crosses and ellipses represent the ±1σ region around the positions in Gaia DR3 (`https://gea.esac.esa.int/archive/`). No reliable signal was found within the range of ±1 arcsec for the other sources, so only dirty images are provided.

Table 2. Phase-referenced positions of two VLBA-detected sources. (Xu et al. 2024)

Source	R.A. (J2000)	Decl. (J2000)	Pos. Error (mas)
J0051B	$00^{\rm h}51^{\rm m}13^{\rm s}.9342632$	$+00°20'47''.177367$	±1.302
J2300A	$23^{\rm h}00^{\rm m}10^{\rm s}.1779370$	$-00°05'31''.586715$	±0.248

$$T_b = 1.22 \times 10^{12}(1+z)\frac{S_\nu}{\theta^2\nu^2} \quad [\rm K] \tag{1}$$

$$L_\nu = 4\pi d_L^2 \frac{S_\nu}{(1+z)^{1+\alpha}} \quad [\rm W/Hz] \tag{2}$$

Two VLBA-detected sources have a significant (∼10 mas) radio-optical positional offset between their VLBA phase-referenced positions and Gaia positions (Fig. 1). They both have significant astrometry excess noise (AEN) in Gaia DR3, similar to "Varstrometry" selected dual AGN (see Section 3). Their Gaia positions could be weighted centers of AGN and host galaxy, and their VLBA positions correspond to the location of black hole. Their significant AEN could be caused by dark Gaia magnitudes and complex galaxy structures.

Based on the pc-scale radio emission properties, we analyzed the 5 GHz radio emission origins in detail for each AGN (Table 3). The radio emission on VLBA scale represents the contribution of pc-scale compact jet. Two VLBA-detected sources both have significant core dominance ($S_{\rm VLBA}/S_{\rm VLA}$>50%). For J2206+0003B and J2300-0005B, their non-detection should be due to insufficient sensitivity of the VLBA, so we cannot determine their jet compactness. The proportion of radio emission originated from the corona is estimated using $L_{\rm R}/L_{\rm X}\sim10^{-5}$ (Güdel & Benz 1993), based on the Chandra X-ray luminosity (Gross et al. 2019), which should be ignored in most targets. The contribution of star formation is estimated through the 1.4 GHz luminosity and Hα luminosity (Fu et al. 2015a). The rest radio emission is thought

to originate from extended jet and wind. The 5 GHz radio emission of almost all targets is jet-dominated, only J2206+0003B is probably dominated by star formation.

Table 3. Emitting region (5 GHz) at the four dual AGN

Source	Compact jet	Extended jet+wind	Corona	Star formation
J0051A	<13%	>64%	–	<23%
J0051B	∼56%	>25%	–	<19%
J2206A	<20%	>47%	∼6%	<27%
J2206B	?	?	–	<72%
J2232A	<51%	>49%	–	–
J2232B	<81%	>19%	–	–
J2300A	∼71%	∼29%	–	–
J2300B	?	?	–	–

From Xu et al. 2024. Question marks represent the unknown proportion based on current observations. En-dashes represent a contribution less than 3%, to be ignored.

The multiband study revealed a possible systematic X-ray deficit similar to Liu et al. (2013) in our small dual-AGN sample (Fig. 2), which could be attributed to the merger-driven tidally induced effect and possibly viewing angle effect. In addition, the [O III] excess originated from star formation could also reduce the X-ray-to-[O III] luminosity ratio. More reliable results depend on the observations and studies involving larger dual-AGN samples.

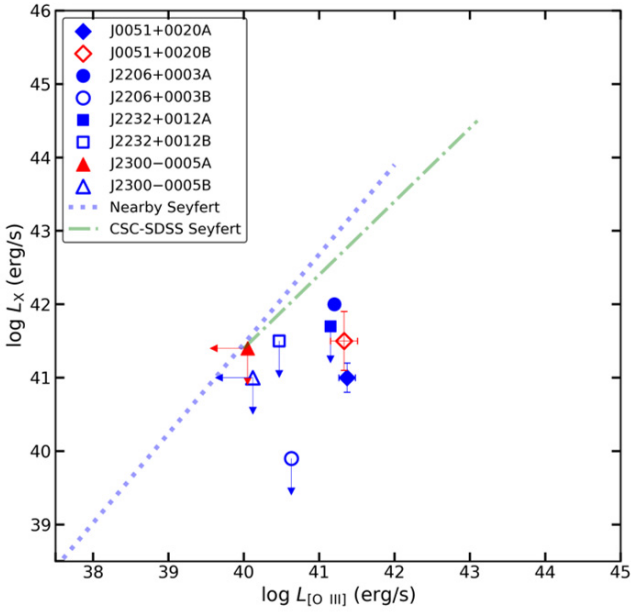

Fig. 2. Unabsorbed rest-frame 2–10 keV X-ray luminosity (L_X) vs. corrected [O III] λ5007 emission-line luminosity ($L_{[O\,III]}$) (Xu et al. 2024). The green dash-dot line represents the relation of Type 2 Seyfert galaxies from the CSC-SDSS cross-match catalogue (Trichas et al. 2012). The blue dot line is the relation for nearby Seyfert galaxies from (Panessa et al. 2006).

3. Peoposed EVN Observations of Varstrometry Selected Dual-Quasar Candidates

Along with Gaia's outstanding astrometric performance and full sky coverage, a novel astrometric technique through photometric variability-induced photocenter pseudo-motion was applied to search for unresolved kpc-scale dual AGN by Hwang et al. (2020), which is named "Varstrometry". This astrometric method is especially suitable for optically unshielded and broad-line AGN, such as quasars. In the case of a dual quasar, these jitters arise from the non-coherent variability of each nucleus, causing the centroid of the total flux to shift. For an off-nucleus quasar, these jitters result from its brightness changing relative to a non-variable host galaxy, causing the centroid of the total flux to shift away from the center of the host galaxy as the flux of the quasar brightens (Chen et al. 2023). The changing photocenter can be well quantified by the parameter *astrometric_excess_noise* (AEN), calculated by *Gaia*'s astrometric solution to describe the disagreement between observations and the best-fitting standard astrometric model. The effectiveness of this method has been confirmed by various observations, and several spatially resolved dual quasar candidates have been identified (e.g. Shen et al. 2021, Chen et al. 2023). It is noted that, the method does not exclude visual dual quasar caused by lensing and projection effects.

Recently, Schwartzman et al. (2024) observed 18 Varstrometry selected dual-quasar candidates using VLA at S and X bands. These candidates were selected from the SDSS quasar catalogue for DR16 and matched with the *Gaia* Early Data Release 3. They have significant AEN (>5σ), high redshifts (z>0.5), and low *Gaia* *G*-band magnitudes (<20) and have clear detection in VLA Sky Survey (VLASS). In the dual-band VLA observations, six candidates exhibit multi-component structures. Among them, three multi-component sources are classified as lensed quasars by spectral analysis, and have faint radio emission (sub-mJy level). One of the six candidates, J0749+2255, has been confirmed as a dual quasar through the Hubble Space Telescope (HST) and VLBA observations (Shen et al. 2021, Chen et al. 2022), indicating the reliability of Varstrometry technique and this dual-quasar sample. The other two dual-quasar candidates, J0111+1713 and J0950+4329, are still lacking further observations and identifications. Their properties are shown in Table 4.

To reveal the fine radio structures and milliarcsec-scale radio emission properties of two Varstrometry selected dual-quasar candidates, we proposed EVN+e-MERLIN observations at 1.6 GHz (project code: EX010A/B). For J0111+1713, its north-east component was observed with the VLBA at C and X bands in snap-shot mode in May 2016, and exhibits a jet structure towards south-west (Fig. 3). We expect to detect the faint component in VLA 10 GHz image of J0111+1713 with our EVN+e-MERLIN deep imaging observations. For another tar-

Table 4. Two varstrometry selected dual-quasar candidates which were proposed for EVN observations

Source (1)	z (2)	G [mag] (3)	AEN (4)	$S_{3\rm GHz}$ [mJy] (5)	$S_{10\rm GHz}$ [mJy] (6)	$\alpha_{\rm power}$ (7)	Sep [arcsec(kpc)] (8)
J0111+1713	2.198	19.29	42.27σ	77.0±0.23	66.8±0.16	-0.09±0.01	0.94(7.96)
				1.76±0.09	3.36±0.14		
J0950+4329	1.771	17.9	139.7σ	2.61±0.06	1.42±0.04	0.08±0.17	0.33(2.86)
				-	0.44±0.02		

Column (1): source name. Column (2): redshift. Column (3): *Gaia* G-band magnitude. Column (4): *Gaia* $astrometric\_excess\_noise$. Column (5): VLA 3 GHz peak flux ± error. Column (6): VLA 10 GHz peak flux ± error. Column (7): spectral index ± error. Column (8): expected AGN-pair separation. (Schwartzman et al. 2024)

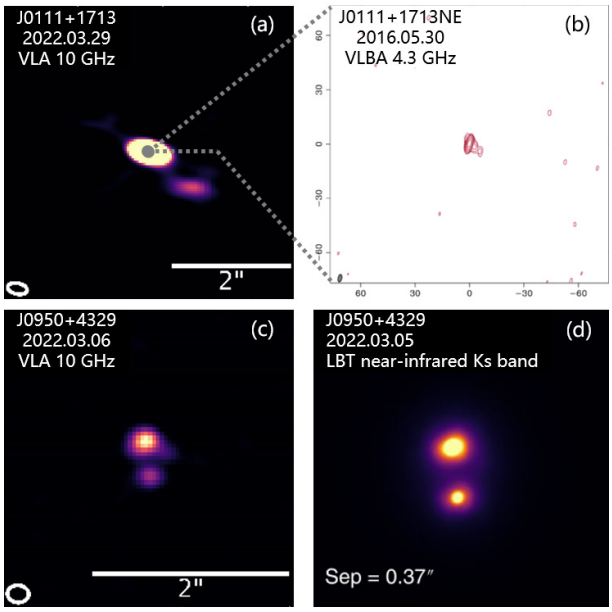

Fig. 3. (a)&(c): VLA 10 GHz images of J0111+1713 and J0950+4329 (Schwartzman et al. 2024). (b): VLBA 4.3 GHz snapshot image of the primary component of J0114+1713 (`https://astrogeo.org/`). (d): LBT near-infrared image of J0950+4329 (Mannucci et al. 2022).

get, J0950+4329, it is also classified as a dual-quasar candidate through *Gaia* Multipeak (GMP) technique (Mannucci et al. 2022), and exhibits dual-core structure in the near-infrared observations with the Large Binocular Telescope (LBT). Our proposed observations will help to confirm the relationship between its two radio cores.

4. Summary and Prospect

We reveal the pc-scale radio emission properties and origins of four dual AGNs in Stripe 82 through VLBA 5 GHz observations. To confirm Varstrometry selected dual-quasar candidates, we proposed 1.4 GHz EVN+e-MERLIN deep imaging observations. In the future, more radio arrays with higher sensitivity, such as FAST Core Array, ngVLA and SKA, will allow us to conduct large-sample dual-AGN search, confirmation and statistical studies.

Acknowledgements. The Very Long Baseline Array is operated by the National Radio Astronomy Observatory, a facility of the National Science Foundation operated under cooperative agreement by Associated Universities, Inc. Scientific results from data presented in this publication are derived from the following VLBA project code(s): BL255A/B. This work has made use of data from the European Space Agency (ESA) mission Gaia (`https://www.cosmos.esa.int/gaia`), processed by the Gaia Data Processing and Analysis Consortium (DPAC; `https://www.cosmos.esa.int/web/gaia/dpac/consortium`).

References

Beasley, A. J., & Conway, J. E. 1995, in ASP Conf. Ser. 82, Very Long Baseline Interferometry and the VLBA, ed. J. A. Zensus, P. J. Diamond, & P. J. Napier (San Francisco, CA: ASP), 327
Chen Y., Hwang H., Shen Y., et al. 2022, ApJ, 925, 162
Chen Y., Liu X., Joseph L., et al. 2023, ApJ, 958, 1
Deller, A., Brisken, W., Phillips, C., et al. 2011, PASP, 123, 275
Di Matteo, T., Springel, V., & Hernquist, L. 2005, Natur, 433, 604
Fu, H., Myers, A., Djorgovski, S., et al. 2015a, ApJ, 799, 72
Fu, H., Wrobel, J., Myers, A., Djorgovski, S., & Yan, L. 2015b, ApJL, 815, L6
Greisen, E. W. 2003, in Information Handling in Astronomy - Historical Vistas, ed. A. Heck (Dordrecht: Kluwer), 109
Gross, A. C., Fu, H., Myers, A. D., Wrobel, J. M., & Djorgovski, S. G. 2019, ApJ, 883, 50
Güdel, M., & Benz, A. O. 1993, ApJL, 405, L63
Hwang H., Shen Y., Nadia Z., et al. 2020, ApJ, 888, 2
Kormendy, J., & Ho, L. C. 2013, ARA&A, 51, 511
Liu, X., Civano, F., Shen, Y., et al. 2013, ApJ, 762, 110
Mannucci F., Pancino E., Belfiore F. & Cicone C., et al. 2022, NatAs, 6, 1185.
Panessa, F., Bassani, L., Cappi, M., et al. 2006, A&A, 455, 173
Schwartzman E., Clarke T. E., Nyland K. & Secrest N. J., et al. 2024, ApJ, 961, 233.
Shen Y., Chen Y. C., Hwang H. C. & Liu X., et al. 2021, NatAs, 5, 569.
Shepherd, M. C. 1997, in ASP Conf. Ser. 125, Astronomical Data Analysis Software and Systems VI, ed. G. Hunt & H. Payne (San Francisco, CA: ASP), 77
Springel, V., White, S. D. M., Jenkins, A., et al. 2005, Natur, 435, 629
Trichas, M., Green, P. J., Silverman, J. D., et al. 2012, ApJS, 200, 17
Xu, W., Cui, L., Liu, X., An, T., et al. 2024, ApJ, 969, 36